Assessment of magnetization reversal and anisotropy of thin films with collapsed hard-magnetization axes through vector magnetometry

H. S. Acosta,[1] A. M. H. de Andrade,[1] L. F. S. Azeredo,[1,2] and J. Geshev[1,*]

[1]*Instituto de Física, Universidade Federal do Rio Grande do Sul, Porto Alegre, 91501-970 Rio Grande do Sul, Brazil*

[2]*Instituto Federal Sul-rio-grandense, Santana do Livramento, 97574-360 Rio Grande do Sul, Brazil*

(Received 14 November 2023; accepted 15 April 2024; published 26 April 2024)

Many magnetic systems display hard-axis collapse—distinct peaks in the remanence and coercivity angular variations, centered 90° off of the easy-magnetization direction. It has recently been discovered that these may also show recoil branches that lie outside the major hysteresis loop. In the present work we examined the magnetization reversal in such systems using vector magnetometry. For Co and Ni films with thickness lower than 25 nm we identified that when the magnetic field is applied in the vicinity of the hard axis and a recoil branch initiates from a state with zero transversal magnetization, the latter remains virtually zero up to the coercive field of the longitudinal component. We showed that this peculiar feature strongly endorses the presumption that these films consist of effectively noninteracting grains in a bidomain magnetic state. We also carried out phenomenological simulations, essential for understanding the magnetization reversal mechanism and anisotropy. Finally, for thin films with collapsed hard axes we presented a simple procedure for evaluating the easy-axis misalignment angle of the bidomain state as well as the anisotropy and intragrain coupling parameters.

DOI: 10.1103/PhysRevB.109.144425

I. INTRODUCTION

Identifying the type of magnetization reversal is of great significance for understanding the behavior of magnetic systems and particularly for the important class of thin ferromagnetic films. Though these are nowadays used in numerous devices, their particular magnetic behavior is still far from being fully understood. A great number of magnetic systems display distinct peaks in the angular variations of their in-plane major hysteresis loops' remanent magnetization, M_{RS}, and coercivity, H_C, centered 90° off of the positions of the respective easy-magnetization directions (see, e.g., Ref. [1] and the references therein). This property is termed hard-axis collapse, HAC [2–4] or hard axis, *HA*, coercivity rocking [5,6]. Recently, it has been discovered that HAC is intrinsically related to a peculiar phenomenon referred to as recoil-curve overshoot, RCO—recoil branches that lie outside the major hysteresis loop [7–9]. Illustrative $M_{RS}(\phi_H)$, where $\phi_H = 0°$ denotes the direction of an in-plane magnetic field **H** parallel to the easy axis, *EA*, is given in Fig. 1, together with respective major and recoil hysteresis loops.

HAC has been attributed to either phase transitions, interface mixing and formation of intermetallic alloys [10], or to ion-induced nonequivalent electronic hybridization between easy and hard magnetization axes [11]. It has been verified that HAC and RCO, presented in Fe, Co, and Ni films, cannot be ascribed to phase transitions or to superpositions of cubic and uniaxial anisotropies [7,8]. These phenomena are well reproduced qualitatively through the model of pairs of exchange-coupled grains with misaligned anisotropy axes proposed by Idigoras *et al.* [2,3]. Analysis and interpretation of experimental and model results [9] have strongly indicated that HAC and RCO originate from grains with magnetizations that split into pairs of exchange-coupled domains with a local *EA* misalignment. The effects of such a splitting are evidenced, essentially, when **H** is applied in the vicinity of *HA*. Both HAC and RCO phenomena should be rather general features of thin films' hysteresis and observed in a variety of systems. Most probably, HAC is not detected and reported more recurrently due to the too great step of ϕ_H ordinarily used in $M_{RS}(\phi_H)$ and $H_C(\phi_H)$ measurements. Thus, the respective magnetization reversal mechanism and anisotropy certainly warrant further investigations which may come out with new applications.

Here we studied the magnetization reversal of Co and Ni films that present HAC and RCO using vector magnetometry. This technique detects simultaneously $M_{\parallel}$ and $M_{\perp}$—the parallel (longitudinal) and perpendicular (transverse) to the direction of **H** components of the spontaneous magnetization, $\mathbf{M_S}$. For a number of thin films we identified a peculiar feature strongly endorsing the presumption that each of these films consists of effectively noninteracting grains in a bidomain magnetic state. We also carried out phenomenological simulations, essential for understanding the reversal mechanism. Finally, we presented a simple procedure for evaluating the *EA* misalignment angle of the bidomain grains and the respective anisotropy and intragrain coupling parameters.

II. EXPERIMENT

Polycrystalline Ta(18 nm)/Ni(t_{Ni})/Ta(18 nm) and Ta(18 nm)/Co(t_{Co})/Ta(18 nm) films with different Ni and Co thicknesses, t_{Ni} and t_{Co}, and also a

*julian@if.ufrgs.br

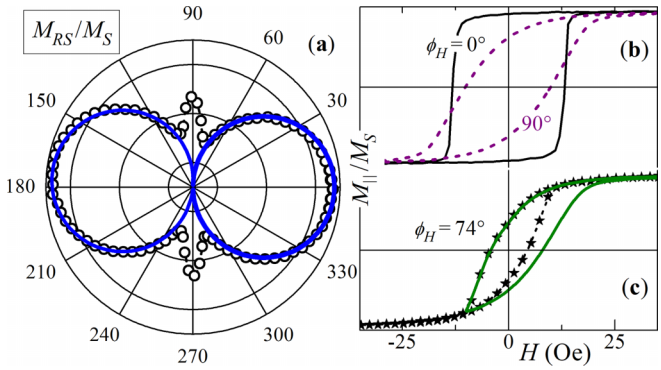

FIG. 1. (a) Major loop's remanent magnetization $M_{RS}(\phi_H)$, obtained for a 20-nm-thick Ni film; the solid line stands for coherent rotation reversal. (b) The corresponding *EA* and *HA* major loops. (c) Major (symbols) and recoil (solid line) loops obtained for **H** applied in the vicinity of the *HA* direction.

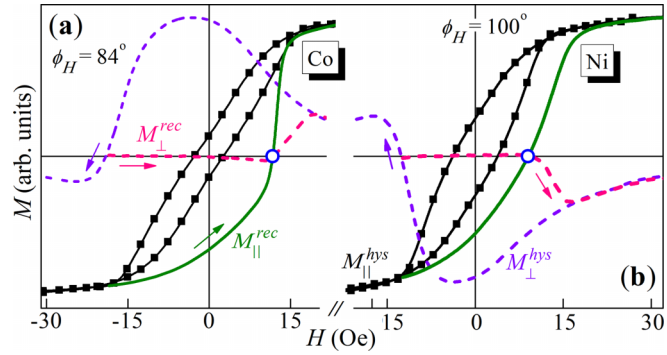

FIG. 2. $M_{||}$ (solid lines) and $M_\perp$ (dashed lines) of the major (symbols) and recoil hysteresis loops measured for **H** applied in the vicinity of the *HA* for (a) Co(20 nm) and (b) Ni(20 nm) films. Only the descending (major loop) and ascending (recoil branch) parts of $M_\perp$ are shown. The empty circles denote the points where $M_{||}(H_C^{\rm rec}) = M_\perp(H_C^{\rm rec}) = 0$.

Ta(18 nm)/Co(10 nm)/IrMn(15 nm)/Ta(18 nm) film were magnetron sputtered at room temperature onto naturally oxidized Si(100) substrates from targets with purity greater than 99.95%. In order to induce uniaxial anisotropy, an in-plane magnetic field of about 1.5 kOe was applied *in situ* during the deposition. Two Co samples were subsequently irradiated at room temperature in a 500 HVEE 70 keV linear accelerator with Ne^+ beams using fluence of 1×10^{15} ions/cm^2 and current density of 100 nA/cm^2 in a 3.5 kOe magnetic field applied along the already-established in-plane *EA*. The Co layer of the Co/IrMn sample was slightly oxidized before the IrMn deposition and no treatment was used to establish exchange bias. The x-ray diffraction patterns show an fcc (111) Ni texture; the Co films present peaks coming from Co fcc (111) and hcp (002) planes, overlapping in a central peak. Details on the structural characterization and on the ion bombardment, IB, can be found elsewhere [7–9].

Room temperature magnetization curves were recorded in-plane via a EZ9 MicroSense vibrating sample magnetometer. The maximum magnetic field values used are higher than the films' anisotropy fields thus ruling out other nonsaturation effects [12–14].

III. RESULTS AND DISCUSSIONS

Magnetic films evidencing HAC may also present RCO. Characterizing our films through vector magnetometry we recognized that, in order to maximize H_C of the recoil branch, the latter has to obey two conditions:

(i) ϕ_H corresponds to one of the $M_{RS}(\phi_H)$ minima;

(ii) the recoil (starting) field, $H_{\rm rec}$, is the field that results in $M_\perp(H_{\rm rec}) = 0$.

Major loops measured for field angles close to such ϕ_H may also present characteristic kinks around $H \approx H_{\rm rec}$, see, e.g., Fig. 3(d). For all thin Co ($t_{\rm Co} \leqslant 25$ nm) and Ni ($t_{\rm Ni} \leqslant 20$ nm) films, we realized that $M_\perp(H)$ of such recoil curves remains virtually zero at least up to the coercive field of $M_{||}$, i.e., $M_{||} = M_\perp = 0$ at $H_C^{\rm rec}$. This very peculiar—and crucial for understanding the magnetic behavior of the systems under consideration—feature is depicted in Fig. 2 for 20-nm-thick Co and Ni films. Figure 3 evidences the same behavior

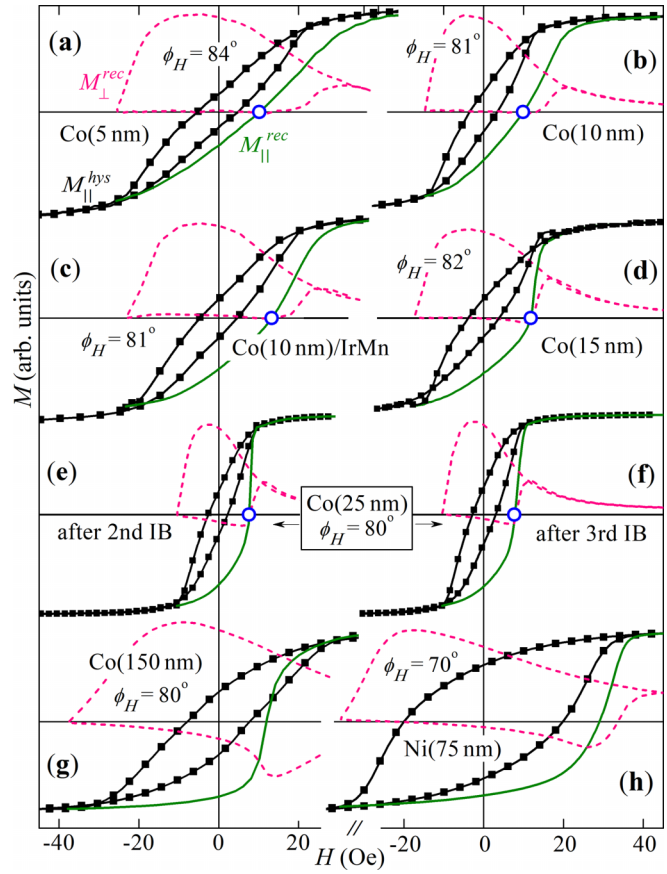

FIG. 3. Major (symbols) and recoil (solid lines) hysteresis loops of ferromagnetic films measured for **H** applied in the vicinity of the *HA*. Panels (a), (b), and (d) present data for 5, 10, and 15-nm-thick Co films, respectively, (c) shows those of the Co(10 nm)/IrMn bilayer, and (e) and (f) give the curves for a 25-nm-thick Co film measured after the second and third subsequent IB. The empty circles denote the points where $M_{||} = M_\perp = 0$. In (g) and (h) are shown data for thick Co and Ni films, where $M_\perp \neq 0$ when the recoil branch's $M_{||} = 0$.

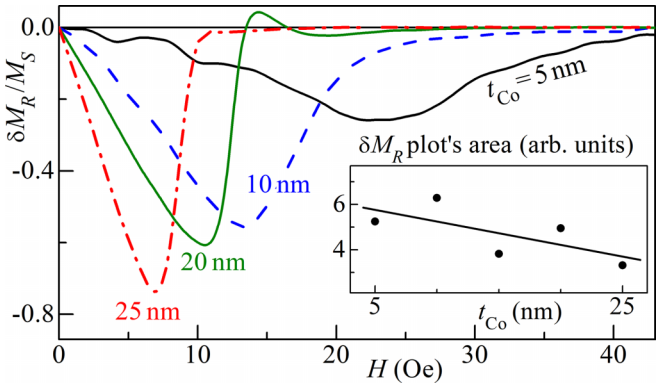

FIG. 4. δM_R plots yielded from the recoil loops of Co films. The inset gives the variation with t_{Co} of the area enclosed by the δM_R curves.

exhibited by the other Co films with $t_{Co} \leqslant 25$ nm. A slight deviation from the zero $M_\perp(H)$ line between H_{rec} and H_C^{rec} is seen in Figs. 3(e) and 3(f) for the 25-nm-thick Co film after each IB. Nevertheless, $M_\perp(H_C^{rec})$ is, again, equal to zero.

It seems established that both HAC and RCO result from exchange coupling. Thus, it is pertinent to inspect the magnetic interaction plots of the films that present $M_\perp(H_{rec}) = M_\perp(H_C^{rec}) = 0$. Figure 4 gives δM_R plots [15–17] yielded from the recoil loops of thin Co films with data shown in Figs. 2 and 3. All plots are virtually negative. Using the classical interpretation, this should be considered as a manifestation of dipolarlike antiparallel coupling. However, positive (parallel) coupling is essentially responsible for the shape and sign of δM_R plots of films with RCO [8]. At first sight, since the amplitude of the plots increases with the Co films' thickness, one might conclude that the coupling strength raises with t_{Co}. Actually, the field region, where the plots show nonzero values, narrows significantly with t_{Co} due to a decrease of the anisotropy field. This results in shrinking of the H interval where the recoil branches lie outside the major loop. Also, the area enclosed by $\delta M_R(H)$ does not decrease considerably with t_{Co} (oppositely to the δM_R's amplitude), as seen in the inset of Fig. 4. These observations suggest that, in our films, the effect of the coupling on $M(H)$ does not depend substantially on t_{Co}.

Aiming to identify the origin of such a distinct magnetization reversal, we carried out numerical simulations employing the model used in our previous work [7]. It considers a pair of exchange-coupled macrospins with magnetizations $\mathbf{M_1}$ and $\mathbf{M_2}$, characterized by uniaxial anisotropies with in-plane anisotropy axes, ea_1 and ea_2, and constants K_1 and K_2, respectively. The directions of ea_1 and ea_2 form angles α_1 and α_2 with the averaged EA of the pair, so the misalignment angle between ea_1 and ea_2 is $\omega = \alpha_1 + \alpha_2$. Due to the film geometry and easy axes aligned within the surface plane, the magnetization rotations occur in the film's plane. The variable part of the system's free magnetic energy, per unit volume, is

$$E = -K_1 \frac{(\mathbf{M_1} \cdot \hat{\mathbf{u}}_\mathbf{1})^2}{M_1^2} - K_2 \frac{(\mathbf{M_2} \cdot \hat{\mathbf{u}}_\mathbf{2})^2}{M_2^2} - J \frac{\mathbf{M_1} \cdot \mathbf{M_2}}{M_1 M_2} - \mathbf{H} \cdot (\mathbf{M_1} + \mathbf{M_2}). \quad (1)$$

The first two terms represent the anisotropy energies (where the versors $\hat{\mathbf{u}}_\mathbf{1}$ and $\hat{\mathbf{u}}_\mathbf{2}$ represent the directions of ea_1 and ea_2, respectively), the third term is the exchange-coupling energy with coupling constant J, and the last term gives the sum of the Zeeman energies. This expression is formally identical to that of Idigoras *et al.* [2,3].

In the simulations, employing a previously developed numerical procedure [18–21], we assumed that $\alpha_1 = -\alpha_2 = \omega/2$, $M_1 = M_2 = M_S$, and $K_1 = K_2 = K$. For such parameters, we reported [7] that the normalized HA remanent magnetization obtained after saturation, $m_{rs}^{ha} = M_{RS}/M_S$, equals $\cos(\frac{\pi}{2} - \frac{1}{2}\arctan\frac{\sin\omega}{\cos\omega - J/K})$. It is straightforward to show that the respective EA remanent magnetization is $m_{rs}^{ea} = \cos(\frac{1}{2}\arctan\frac{\sin\omega}{\cos\omega + J/K})$. Using the former expression one obtains, for $m_{rs}^{ha} \neq 1$, the ratio between the exchange coupling $H_E (= J/M_S)$ and anisotropy $H_U (= 2K/M_S)$ fields:

$$\frac{2H_E}{H_U} = \sin\omega \cot\left(2\arccos m_{rs}^{ha}\right) + \cos\omega. \quad (2)$$

The same ratio can be derived from the m_{rs}^{ea} expression

$$\frac{2H_E}{H_U} = \sin\omega \cot\left(2\arccos m_{rs}^{ea}\right) - \cos\omega, \quad (3)$$

valid for $m_{rs}^{ea} \neq 1$. The above two relations could be used for determining some characteristics of real systems.

Representative major and recoil hysteresis loops, calculated for both cases of exchanged coupled and non-interacting $\mathbf{M_1}$ and $\mathbf{M_2}$ for $\mathbf{H}$ applied near the HA direction are shown in Fig. 5. It is important to emphasize here that, when analyzing the simulated curves, we surveyed the variations of both longitudinal and transverse components of $\mathbf{M_1}$ and $\mathbf{M_2}$ as H is varied, resulting in precise identification of their reversal. The arrows in Fig. 5 depict the orientations of $\mathbf{M_1}$ and $\mathbf{M_2}$ at representative states of the ascending branches of all loops; arrows of the descending branch of the recoil loop for $J = 0$ are also shown in Fig. 5(b).

The magnetization curves corresponding to the pair of noninteracting macrospins carry out all characteristics one would expect. The reversal of $\mathbf{M_1}$ and $\mathbf{M_2}$ obeys the coherent Stoner-Wohlfarth, SW, model [22]. The recoil loop lies inside the major one. Even the crossing of the ascending and descending branches of one of the macrospins, predicted by the SW model, is noticeable. An important feature for the present work is the spins' configuration at the major-loop's coercive field state where $M_\parallel(H_C) = 0$, resulting in $M_{\parallel,1} = -M_{\parallel,2}$. For a system consisting of only two macrospins, this also requires $M_{\perp,1} = -M_{\perp,2}$ since none of the spins, which rotate in opposite directions, has rotated irreversibly as H is varied from saturation to H_C. Symmetry or energy considerations attest that, at this state, the direction of the antiparallel $\mathbf{M_1}$ and $\mathbf{M_2}$ is that of the system's EA, regardless the value of ω. The corresponding arrows' configurations are denoted in Figs. 5(a) and 5(b) for the coercive-field states of the major loop, H_C^- and H_C^+.

The characteristics of the model hysteresis loops of the pair of coupled macrospins are rather different. It is clearly seen in Fig. 5(c) that $\mathbf{M_1}$ and $\mathbf{M_2}$ rotate nearly in unison. This results in saturation remanence and coercivity values lower

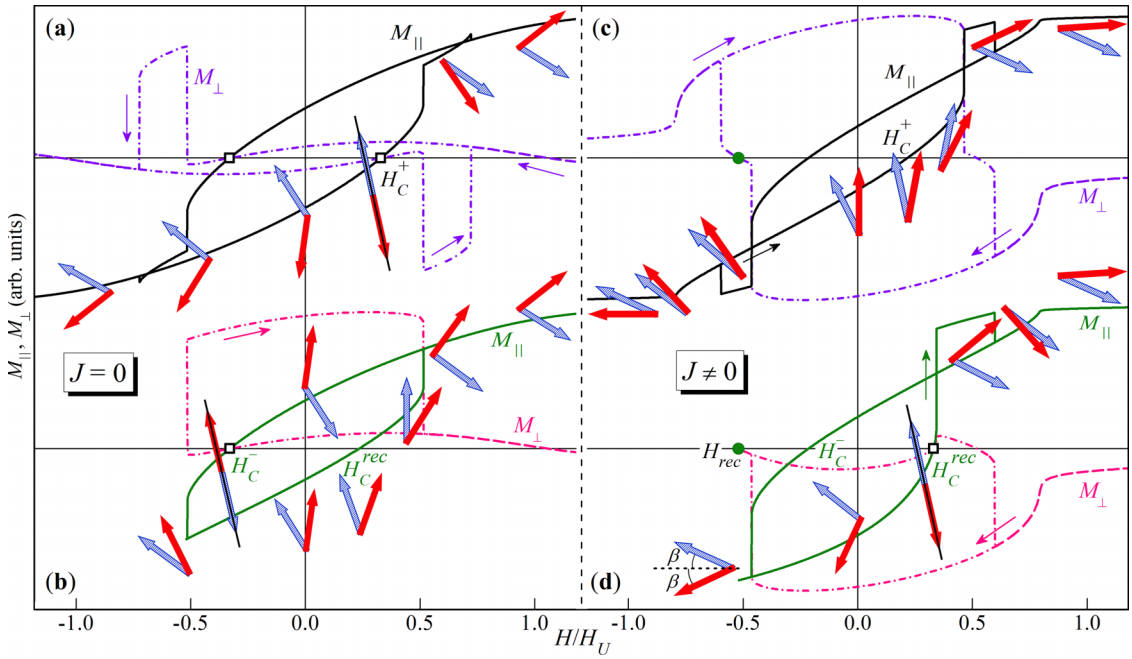

FIG. 5. $M_\parallel$ (solid lines) and $M_\perp$ (dash dotted lines) of the major (top panels) and recoil (bottom panels) hysteresis loops. These are obtained through the model which considers two macrospins with misalignment angles of their easy axes (in relation to the averaged *EA*) $\alpha_1 = -\alpha_2 = 20^\circ = \omega/2, M_1 = M_2 = M$, and $K_1 = K_2 = K$. The other parameters used are $\phi_H = 103^\circ, K/M_S = 25\,\text{Oe}, J/K = 0$ (left panels), and $J/K = 0.6$ (right panels). The arrows indicate the orientations of $\mathbf{M_1}$ and $\mathbf{M_2}$ at representative states of the ascending branches of the loops; arrows of the descending branch of the recoil loop in (b) are also shown. The full circles in (c) and (d) correspond to the starting point of the recoil branch (where $M_\perp = 0$) when $J \neq 0$; the empty squares represent the coercive-field states of the major loop for $J = 0$ as well as that of the recoil branch for $J \neq 0$.

than those of the noninteracting system, as expected. The kink observed shortly before positive saturation occurs in the only field region of the descending branch of the major loop where $\mathbf{M_1}$ and $\mathbf{M_2}$ are not almost parallel. Due to the exchange coupling, one of the macrospins is "dragged" to reverse earlier to this frustrated state. The midpoint of this kink corresponds to the "coercive field" of $M_\perp$ where $M_{\perp,1} = -M_{\perp,2}$ while $M_{\parallel,1} = M_{\parallel,2}$, i.e., the macrospins make acute angles, $+\beta$ and $-\beta$, with $\mathbf{H}$, and the normalized to M_S system's magnetization is equal to $\cos\beta$. Further increase of H extinguishes this frustrated state and both $\mathbf{M_1}$ and $\mathbf{M_2}$ rotate, again nearly in unison, toward saturation.

Figure 5(d) shows a model recoil curve with H_{rec} equal to the field of the midpoint of the kink of the descending branch of the major loop. As H (negative) is decreased, the two macrospins rotate in opposite directions. When $H = 0$, both macrospins contribute significantly to the remanent magnetization, which is much greater than that of the respective major loop—hence RCO. As $\mathbf{H}$ is reversed and its magnitude is gradually increased, $\mathbf{M_1}$ and $\mathbf{M_2}$ continue to rotate, one clockwise and the other counterclockwise, reaching an antiparallel configuration at the coercive field state. This configuration also implies $M_{\perp,1}(H_C^{\text{rec}}) = -M_{\perp,2}(H_C^{\text{rec}})$. Again, using symmetry considerations and/or identifying the minimum energy requirements for this interacting state, one obtains that the direction of the antiparallel $\mathbf{M_1}$ and $\mathbf{M_2}$ is the same as that of the system's *EA*. Thus, $H_C^{\text{rec}}(J \neq 0)$ equals that of the major loop of the noninteracting case, $H_C(J = 0)$. However, $H_C(J = 0) > H_C(J \neq 0)$, substantiating the observation of maximum recoil curve's coercivity at these exact experimental conditions.

The significance of such a remarkable result is much greater. Note that this outcome—the common direction of the antiparallel macrospins is that of their averaged *EA* at the $H_C^{\text{rec}}(J \neq 0)$ state—does not depend on ω. This means that even considering a great number of pairs of coupled macrospins with different misalignment angles, both $M_\parallel$ and $M_\perp$ of the system will be equal to zero at H_C^{rec}. The averaged *EA*s of all pairs having one and the same direction is expected to take place after in-field film growth, annealing, or IB. The value of $H_C^{\text{rec}}(J \neq 0)$ for such an agglomerate of macrospins does not depend on their misalignment angles as well, and equals that of a single SW macrospin for the particular value of ϕ_H.

Our experiments showed that the RCO characteristics are optimized when H_{rec} is the field yielding $M_\perp(H_{\text{rec}}) = 0$. Moreover, $M_\perp(H)$ of such recoil branches remains practically zero up to H_C^{rec} for a number of thin films. These results, together with the model ones, strongly indicate that the particular feature, i.e., recoil loops with $M_\perp(H_{\text{rec}}) = M_\perp(H_C^{\text{rec}}) = 0$, is a characteristic of films consisting of pairs of macrospins with (most probably) different misalignment angles though one and the same average *EA* direction. These remarkable characteristics allow estimating the anisotropy and coupling parameters of such systems as shown below.

The angular variation of M_{RS} of the Ni film shown in Fig. 1(a) coincides, practically, with the one calculated in the framework of the SW model [22], excluding the field orientations near the *HA* one. This, usually considered as evidence for a magnetization behavior of a single macrospin rotating coherently, has also been observed for a number of different systems including films presenting HAC or RCO [7,8]. We obtained that $M_{RS}(\phi_H)$ curves, calculated for pairs of coupled macrospins like those presenting RCO and considered here, are virtually identical with the SW one for ϕ_H aside of the HAC region, i.e., on the demagnetization part of the major loop, nearly in unison rotation of $\mathbf{M_1}$ and $\mathbf{M_2}$ dominates for the majority of field orientations, mimicking a SW reversal.

The recoil loops of Ni and Co films thicker than 25 nm do not show the particularity $M_\perp(H_{\rm rec}) = M_\perp(H_C^{\rm rec}) = 0$ that the thinner films exhibit, see Figs. 3(e) and 3(f). This should naturally be attributed to the presence of grains of greater sizes in the thicker films as our previous study has established—the average size raises from approximately 4 to 17 nm as $t_{\rm Co}$ increases from 5 to 150 nm, and from 16 and 31 nm for $t_{\rm Ni}$ varying from 20 and 75 nm [7]. With the increase of the grain size, a bidomain magnetic state is no longer energetically favorable so such grains are in multidomain states. Surely, $M_\perp(H)$ variations of these grains are dissimilar from the bidomain ones.

The uniaxial anisotropy field of SW-like systems showing nearly zero *HA* remanence and coercivity can be considered to be equal to the field corresponding to the maximum of the $M_\parallel$'s field derivative in the *HA* curve (see, e.g., Ref. [23]), where it is expected that only coherent rotation takes place. This procedure cannot be applied if *HA* is collapsed. Below we present a method allowing the evaluation of not only H_U but also of H_E and ω for systems with recoil branches characterized by $M_\perp(H_{\rm rec}) = M_\perp(H_C^{\rm rec}) = 0$.

Equations (2) and (3) give relations between m_{rs}^{ea} and m_{rs}^{ha}, obtained from the experiment, and the unknown parameters ω, H_E and H_U. From these equations, one derives an expression for ω in terms of $m_{rs}^{ea} \neq 1$ and $m_{rs}^{ha} \neq 1$, i.e.,

$$\omega = \text{arccot}\frac{\cot\left(2\arccos m_{rs}^{ea}\right) - \cot\left(2\arccos m_{rs}^{ha}\right)}{2} \qquad (4)$$

for $m_{rs}^{ea} \neq m_{rs}^{ha}$. Yet another independent relation between the latter can be found examining the equilibrium when $M_\perp(H_{\rm rec}) = 0$. In this particular state, the configuration of $\mathbf{M_1}$ and $\mathbf{M_2}$ is the one shown in Fig. 5(d), where $M_{\perp,1} = -M_{\perp,2}$ and $M_{\parallel,1} = M_{\parallel,2}$, i.e., each of these spins forms one and the same angle $\beta = \arccos m_{\rm rec}$ with $\mathbf{H}$, where $m_{\rm rec}$ is the normalized to M_S value of $M_\parallel$. The equilibrium's examination through the first and second derivatives of the energy given by Eq. (1) results in

$$\frac{2H_E}{H_U}\sin(-2\beta) = \frac{2H_{\rm rec}}{H_U}\sin\beta + \cos(2\phi_H)\sin(2\beta+\omega). \qquad (5)$$

Given that β, $H_{\rm rec}$, and ϕ_H also come also from the experiment, Eqs. (2)–(5) allow a direct estimation of ω, H_E, and H_U. First, one obtains ω from Eq. (4), then the ratio H_E/H_U can be evaluated by substituting the obtained value for ω in either Eq. (2) or Eq. (3). Subsequently, using the values of ω and H_E/H_U, and the experimental ones (ϕ_H, $H_{\rm rec}$ and $m_{\rm rec}$) in Eq. (5), one calculates H_U and, finally, H_E. In case the M_S value is known, one can also obtain the values of J and K.

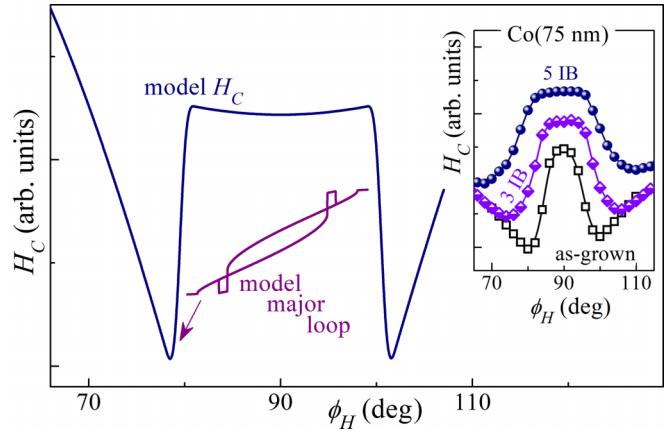

FIG. 6. Model $H_C(\phi_H)$ for $\mathbf{H}$ applied near the *HA* direction, obtained employing $\omega = 38°$, $H_U = 62$ Oe, and $H_E = 20$ Oe, values estimated through Eqs. (3)–(5) and experimental data ($m_{rs}^{ea} = 0.98$, $m_{rs}^{ha} = 0.63$, $m_{\rm rec} = 0.87$, $H_{\rm rec} = 26$ Oe, and $\phi_H = 84°$) of the 5-nm-thick Co film. A major hysteresis loop calculated with these parameters and ϕ_H of the minimum of the model H_C vs ϕ_H curve is also plotted. The inset gives the experimental $H_C(\phi_H)$ in the *HA* region for a 75-nm-thick Co film measured after the in-field growth and also after three and five subsequent Ne ion bombardments.

Adopting the above modus operandi, we estimated, as an example, ω, the anisotropy field and coupling field to be $\omega \approx 38°$, $H_U \approx 62$ Oe, and $H_E \approx 20$ Oe for the 5-nm-thick Co film with data presented in Fig. 3(a). These values for ω, H_U and H_E should be considered as typical for the most representative grains of the particular polycrystalline film (in fact, the same supposition is utilized when estimating K of a regular SW-like system with noncollapsed *HA*). Using these parameters, we calculated the $H_C(\phi_H)$ curve and the major hysteresis loop for $\mathbf{H}$ applied in the HA vicinity shown in Fig. 6. As should be expected, due to the simplicity of the model and the complexity of the real polycrystalline film, the quantitative agreement between model and experiment is not very good. Nonetheless, the hysteresis loop presents RCO and $H_C(\phi_H)$ shows HAC. Though the plateaulike shape of the model $H_C(\phi_H)$ curve near the *HA* position might seem peculiar, the inset in Fig. 6 demonstrates that films showing RCO could actually present very similar $H_C(\phi_H)$ variations. In the inset, the evolution of $H_C(\phi_H)$ in the *HA* region with the IB of a Ta/Co(75 nm)/Ta film is shown. It is clearly seen that, as a result of the IB, the $H_C(\phi_H)$ curve evolves to one with a plateaulike shape similar to the model one. The reason for such a transformation is, most probably, an eradication of the greater, multidomain Co grains which do not contribute to the collapse due to mixture at the Ta/Co and Co/Ta interfaces [9]. As a result, the effective thickness of the magnetic layer decreases and the relative amount of Co contributing to HAC raises, thus explaining the enhanced resemblance between model and experimental curves.

In summary, we examined, through vector magnetometry, the magnetization reversal of magnetic films that present hard-axis collapse and recoil-curve overshoot. We observed that, in order to maximize the value of $H_C^{\rm rec}$, the magnetic field

orientation should correspond to the minimum of $M_{RS}(\phi_H)$ and the transverse magnetization component $M_\perp(H_{\rm rec})$ should be zero. We then discovered a particular feature—for this configuration $M_\perp(H)$ remains virtually zero at least up to $H_C^{\rm rec}$. Model simulations, essential for understanding the magnetization reversal mechanism and anisotropy, endorsed the presumption that each of these films consists of effectively noninteracting grains in a bidomain magnetic state. Finally, we presented a method for evaluating the easy-axis misalignment angle together with the anisotropy and intragrain coupling parameters of the most representative grains for thin films with collapsed hard axes.

ACKNOWLEDGMENTS

This work was supported by the Brazilian agencies CNPq (Grants No. 313624/2020-8, No. 406009/2021-0, and No. 309125/2022-7), FAPERGS (Grant No. 21/2551-0002019-9) and CAPES. The sputtering deposition was performed at LCN and the ion irradiation at LII, both at IF-UFRGS.

[1] K. P. Leib, K. Zhang, G. A. Müller, R. Gupta, and P. Schaaf, Hyperfine Interact. **160**, 39 (2005).
[2] O. Idigoras, A. K. Suszka, P. Vavassori, P. Landeros, J. M. Porro, and A. Berger, Phys. Rev. B **84**, 132403 (2011).
[3] O. Idigoras, A. K. Suszka, P. Vavassori, B. Obry, B. Hillebrands, P. Landeros, and A. Berger, J. Appl. Phys. **115**, 083912 (2014).
[4] M. Sedrpooshan, H. Ahmadvand, D. L. González, and S. van Dijken, Phys. Rev. B **98**, 214444 (2018).
[5] C. Mathieu, V. R. Inturi, and M. J. Hadley, IEEE Trans. Magn. **44**, 432 (2008).
[6] V. Inturi, H. Yin, M. Kief, M. Hadley, and C. Mathieu, IEEE Trans. Magn. **48**, 1718 (2012).
[7] J. Geshev, W. J. S. Garcia, V. Z. C. Paes, L. F. S. Azeredo, L. S. Dorneles, and A. M. H. de Andrade, Phys. Rev. B **104**, 054436 (2021).
[8] J. Geshev and A. M. H. de Andrade, J. Magn. Magn. Mater. **560**, 169573 (2022).
[9] L. F. S. Azeredo, J. Geshev, P. L. Grande, and A. M. H. de Andrade, Phys. Rev. B **107**, 134428 (2023).
[10] K. Zhang, R. Gupta, G. A. Müller, P. Schaaf, and K. P. Lieb, Appl. Phys. Lett. **84**, 3915 (2004).
[11] G. S. Chang, A. Moewes, S. H. Kim, J. Lee, K. Jeong, C. N. Whang, D. H. Kim, and S.-C. Shin, Appl. Phys. Lett. **88**, 092504 (2006).
[12] J. Geshev, L. G. Pereira, and V. Skumryev, Phys. Rev. Lett. **100**, 039701 (2008).
[13] J. Geshev, J. Phys.: Condens. Matter **21**, 078001 (2009).
[14] A. Harres, M. Mikhov, V. Skumryev, A. M. H. de Andrade, J. E. Schmidt, and J. Geshev, J. Magn. Magn. Mater. **402**, 76 (2016).
[15] J. Geshev, J. Magn. Magn. Mater. **467**, 135 (2018).
[16] J. Geshev, L. L. Bianchi, R. F. Lopes, J. L. Salazar Cuaila, A. Harres, J. Magn. Magn. Mater. **497**, 166061 (2020).
[17] J. Geshev, R. F. Lopes, J. L. Salazar Cuaila, L. L. Bianchi, A. Harres, J. Magn. Magn. Mater. **500**, 166420 (2020).
[18] J. Geshev, O. Popov, V. Masheva, and M. Mikhov, J. Magn. Magn. Mater. **92**, 185 (1990).
[19] V. Masheva, J. Geshev, and M. Mikhov, J. Magn. Magn. Mater. **137**, 350 (1994).
[20] A. Harres and J. Geshev, J. Phys.: Condens. Matter **23**, 216003 (2011).
[21] G. Salazar-Alvarez, J. Geshev, S. Agramut-Puig, C. Navau, A. Sánchez, J. Sort, and J. Nogués, ACS Appl. Mater. Interfaces **8**, 22477 (2016).
[22] E. C. Stoner and E. P. Wohlfarth, Philos. Trans. R. Soc. London, Ser. A **240**, 599 (1948).
[23] M. A. Arranz, J. M. Colino, and F. J. Palomares, J. Appl. Phys. **115**, 183906 (2014).